Lithos 332–333 (2019) 55–66

Contents lists available at ScienceDirect

Lithos

journal homepage: www.elsevier.com/locate/lithos

Seismicity in Cascadia

Michael G. Bostock *, Nikolas I. Christensen, Simon M. Peacock

Department of Earth, Ocean and Atmospheric Sciences, The University of British Columbia, Canada

ARTICLE INFO

Article history:
Received 11 July 2018
27 December 2018
Accepted 23 February 2019
Available online 26 February 2019

Keywords:
Seismicity
Tremor
Cascadia
Fluids
Subduction
Forearc
Serpentinization
Eclogitization
Volcanism

ABSTRACT

We examine spatio-geometric patterns in the density of seismicity within the Cascadia forearc to gain insight into controls on seismogenesis. Tremor epicenters exhibit the most regular distribution defining a 40–80 km wide band extending along almost the entire convergent margin from the southern terminus of Gorda plate subduction in northern California to the central Explorer plate below northern Vancouver Island. Based on prior characterization of constituent low-frequency earthquakes, the up- and down-dip limits of tremor are assumed to represent slab isodepth contours at nominal values of 28 and 45 km, between which fluids at near-lithostatic overpressures are trapped within the subducting slab. Epicenters of earthquakes within the North American crust are anticorrelated with those of tremor, and concentrated in Washington and northern California where they are sandwiched between tremor and the Cascade volcanic arc. Seismicity within the subducting plate possesses the most limited epicentral distribution. Seismicity is confined to shallow depths off Vancouver Island and in northern California, and projects to greater depths beneath Washington and southern British Columbia. Comparison of seismicity patterns with long-wavelength slab geometry and thermo-petrologic constraints suggests that seismicity occurrence in Cascadia is governed by an interplay between slab strain, metamorphic dehydration within the subducting oceanic plate, and a plate boundary seal that controls where fluids enter the overriding plate. The inferred fluid evolution model harbors interesting implications for mantle wedge hydrology, forearc crustal composition and volcanism in Cascadia and other warm subduction zones.

1. Introduction

Cascadia is unusual among subduction zones in its low levels of seismicity and absence of megathrust earthquakes in historic times. Indeed, the case for active subduction was debated for almost a decade after the advent of plate tectonic theory (Riddihough and Hyndman, 1976), and the question of aseismic versus seismogenic slip on the plate boundary thrust persisted for longer still (Heaton and Kanamori, 1984; Rogers, 1988). The true seismogenic potential of the Cascadia megathrust was established in a detective story involving multiple lines of evidence (e.g., Adams, 1990; Atwater, 1987; Hyndman and Wang, 1993; Satake et al., 1996) pointing irrevocably to a history of large thrust events, culminating most recently with a M ~ 9 event on the evening of January 26, 1700. Since modern recording began, the megathrust interface has been disquietingly calm with rare occurrences of microearthquakes offshore. These events were initially detected off the Oregon coast (Trehu et al., 2008) with more recent catalogues from ocean bottom deployments indicating low levels along the entire Cascadia offshore margin (Stone et al., 2018). Although there has been a complete absence of recorded regular seismicity along onshore portions of the plate boundary during this period, a new class of seismicity intimately associated with slow slip (Dragert et al., 2001) is now known to occur down-dip of the inferred megathrust seismogenic zone at regular (~1 year) intervals (Rogers and Dragert, 2003), along the entire margin (e.g., Brudzinski and Allen, 2007). This phenomenon is known as tectonic tremor or, collectively, as episodic tremor and slip (ETS). Away from the plate boundary, regular seismicity is catalogued within the subducting Juan de Fuca plate and in the crust of the overriding North American plate but in a non-uniform geographical distribution with concentrations off western Vancouver Island, in the Puget Sound region and in northern California (see, e.g., Ludwin et al., 1991; Rogers and Horner, 1991; Uhrhammer, 1991; and references therein; see also Fig. 1 for a map indicating key geographic locations and tectonic features). Factors that contribute to this pattern have been long debated with a growing consensus that slab pull, plate geometry and metamorphic dehydrations all play roles, in particular, for slab earthquakes (e.g., McCrory et al., 2012; Wada et al., 2010). It has also been noted that tremor displays a tendency toward anticorrelation in epicentral distribution with regular seismicity (e.g., Boyarko and Brudzinski, 2010; Kao et al., 2009). Our focus in this study is to further consider the distribution of tremor, its spatio-geometric relations with other forms of seismicity and the physical conditions under which it occurs. These factors yield further insights into the nature of both slab and crustal seismicity in the Cascadia forearc with a number of interesting, more general implications.

* Corresponding author.
E-mail address: bostock@eos.ubc.ca (M.G. Bostock).

https://doi.org/10.1016/j.lithos.2019.02.019
0024-4937/

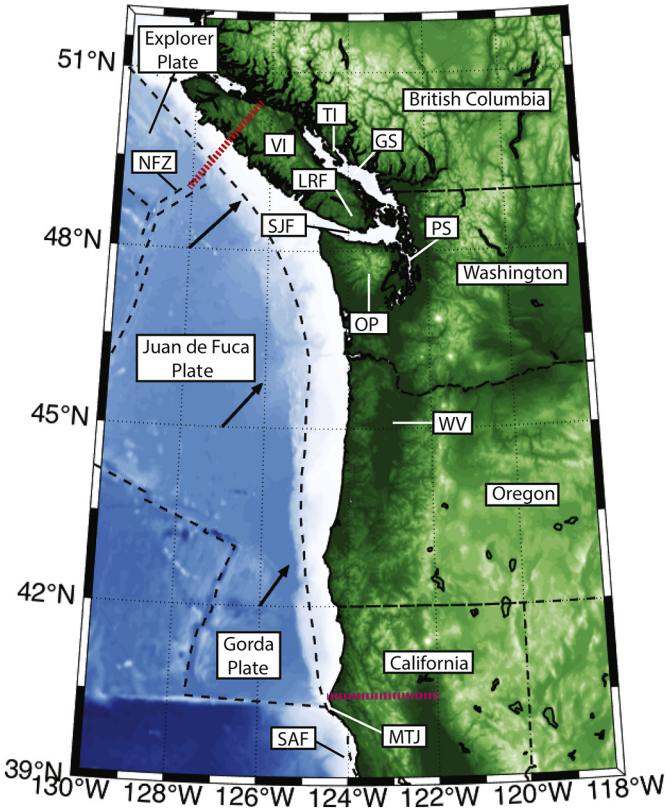

Fig. 1. Map of geographic locations and tectonic features referred to in text. Labels are GS: Georgia Strait, MTJ: Mendocino Triple Junction, NFZ: Nootka Fault Zone, LRF: Leech River Fault, OP: Olympic Peninsula, PS: Puget Sound, SAF: San Andreas Fault, SJF: Strait of Juan de Fuca, TI: Texada Island, VI: Vancouver Island, WV: Willamette Valley. Plate boundaries are shown as dashed lines, and the locations of the two seismicity profiles in Fig. 8 are shown as colored dotted lines (NFZ in red, MTJ in magenta).

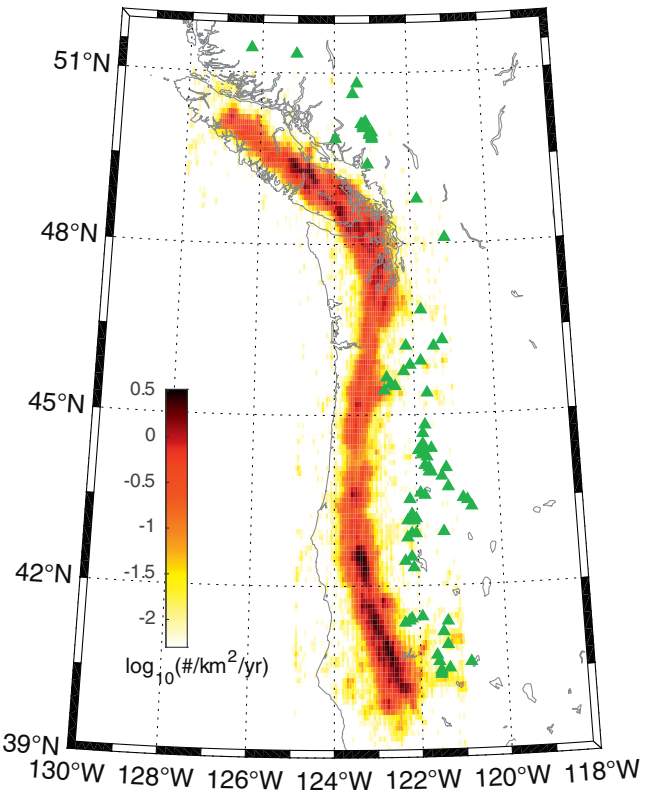

Fig. 2. Tremor density (base 10 logarithm of number of detections per square kilometer per year) distribution along the Cascadia margin. Green triangles represent locations of volcanic centers.

2. Spatial patterns in Cascadia seismicity

We begin our analysis with a consideration of the spatial distribution of seismicity along the Cascadia forearc. In particular, we divide seismicity into three classes: tremor, crustal earthquakes, and slab earthquakes. To illuminate details in the patterns of their distributions we apply a kernel density estimator (Botev et al., 2010) to epicentral data from relevant earthquake catalogues.

2.1. Tremor

Tectonic tremor was discovered <2 decades ago in Japan (Obara, 2002) and documented shortly afterwards in Cascadia in association with slow slip, where the two phenomena were originally dubbed ETS (Rogers and Dragert, 2003). Despite its poorly understood and enigmatic nature, tremor possesses the most regular epicentral distribution of the 3 classes of seismicity we shall consider. This behavior is illustrated in Fig. 2 where we display tremor density using the catalog of Wech (2010) for the period August 2009 – January 2018. Tremor extends along almost the full length of the Cascadia margin from northern Vancouver Island to northern California. In particular, the along-strike limits of subduction are clearly demarcated in the north by the subduction of southern and central portions of the Explorer plate in northern Vancouver Island (Riddihough, 1977) and at the southern terminus of Gorda plate subduction in northern California (McCrory et al., 2012). The tremor epicentral zone width averages approximately 60 km from a minimum width of ~40 km beneath the Columbia River to a maximum width of ~80 km beneath the Strait of Juan de Fuca. Tremor density appears strongest in northern California and along southern Vancouver Island and northern Washington.

On seismograms, tremor is an emergent and bandlimited (2–8 Hz) signal that is most readily recognized through the similarity and systematic moveout of waveform envelopes across local seismograph networks. As a consequence, temporal resolution of waveform correlation is limited and hypocentral depths are considerably more difficult to constrain than epicenters. However, with careful signal processing, individual elements of tremor known as low frequency earthquakes (LFEs) that display clear P- and S- arrivals can be isolated and precisely mapped to depth (Shelly et al., 2006). In Cascadia and elsewhere, LFEs appear to lie within a narrow depth interval (≤ 1–2 km) with polarizations that are consistent with thrust motion on a shallow dipping plate interface (Armbruster et al., 2014; Royer and Bostock, 2014). On the basis of this observation and others that are detailed in section 3.2, we will henceforth assume (as is common, though not universal, cf. Kao et al., 2009) that tremor is effectively isolated to a plate boundary shear zone dipping between depths of approximately 28 and 45 km, that vary only slightly along the margin (e.g., Plourde et al., 2015; Royer and Bostock, 2014; Thomas and Bostock, 2015).

2.2. Crustal seismicity

To examine the distributions of regular seismicity landward of the deformation front, we combine regional seismicity catalogues from U.S. regional networks (University of Washington, 1963; USGS Menlo Park, 1967) and the Geological Survey of Canada (1989) between January 1984 and January 2018, taking care to remove duplicate events. We limit our attention to magnitudes $M_L \geq 1$ as an estimate of completeness threshold over the region to minimize spatial sampling bias. North of California, we assign hypocenters above 26 km depth to the North American crust and those below 30 km depth to the subducting Juan

de Fuca plate (we note that close to the deformation front this division may result in some erroneous mapping of shallow intraslab events into the crust). In northern California (south of 42° N) where shallow slab structure is complicated but the slab surface is precisely determined by double-difference hypocentral relocation, we apply the McCrory et al. (2012) slab model to the double difference catalog of Waldhauser (2018) to separate crustal from slab seismicity. The crustal seismicity catalog thus assembled comprises a total of 97,181 epicenters with a density distribution plotted in Fig. 3. In addition, we superimpose the external contour of the tremor distribution from Fig. 2 in black to provide further spatial reference.

As has been previously noted in regional studies of northern (Kao et al., 2009) and southern (Boyarko and Brudzinski, 2010) Cascadia, epicenters of tremor and crustal earthquakes display a strong tendency to spatial anticorrelation. In northern Cascadia, increased levels of seismicity are most apparent in Washington where seismicity is largely sandwiched between the down-dip tremor limit and the Cascade arc. There is minor overlap along Puget Sound where a network of larger crustal faults has been documented (e.g., Blakely et al., 2011). Much of the forearc seismicity in this region is swarm-like, occurring over periods of years to decades, and clustered, frequently as sub-vertical hypocenter streaks with dimensions of 5–10 km (Balfour et al., 2012; Savard et al., 2018). Forearc crustal seismicity drops markedly through Oregon and reappears strongly expressed in northern California, again largely skirting the envelope of tremor epicenters, except at the very southern limit of tremor where tremor underlies deformation associated with the northern end of the San Andreas fault system. North of Washington, seismicity also drops though low levels follow the trend of the British Columbia volcanoes, diverging northward with the down-dip limit of tremor. On the up-dip side of tremor, crustal seismicity is most pronounced at the northern and southern margins of the subduction zone. Above the underthrusting Explorer plate, concentrations of crustal events occur off Brooks Peninusula and above the subducting Nootka fault zone that forms the southeastern boundary with the Juan de Fuca plate (e.g., Hyndman et al., 1979; Obana et al., 2014). In the latter case, seismicity approaches, but does not overlap significantly, the up-dip limit of tremor. In like manner, there is a concentration of crustal seismicity above the southern edge of the subducting Gorda plate immediately north of Cape Mendocino (McCrory et al., 2012) and seaward of the up-dip tremor limit.

2.3. Intraslab seismicity

Of the three seismicity classes, intraslab (within the subducting plate) seismicity exhibits the most limited geographical distribution although it mimics the geometry of crustal seismicity to some degree, as evident from Fig. 4. Events deeper than 40 km are largely restricted to the Puget Sound and parts landward, with a localized earthquake ``nest" at depths between 60 and 70 km below the Georgia Strait, southeast of Texada Island (Merrill and Bostock, 2018). Unlike crustal seismicity, there is a significant epicentral overlap between deep intraslab events and tremor occurrence below the eastern Strait of Juan de Fuca and southward. Shallow intraslab seismicity (≤ 35 km depth) in northern Cascadia is most strongly expressed along the west coast of Vancouver Island with local concentrations off Nootka Island (subsurface extension of the Nootka fault), beneath Barkley Sound, and the northwestern corner of the Olympic Penisula (Rogers, 1983). These events parallel the up-dip limit of tremor with some minor overlap. Intraslab events are infrequent below Oregon, but reappear in a similar pattern within the subducting Gorda Plate near the Mendocino triple junction

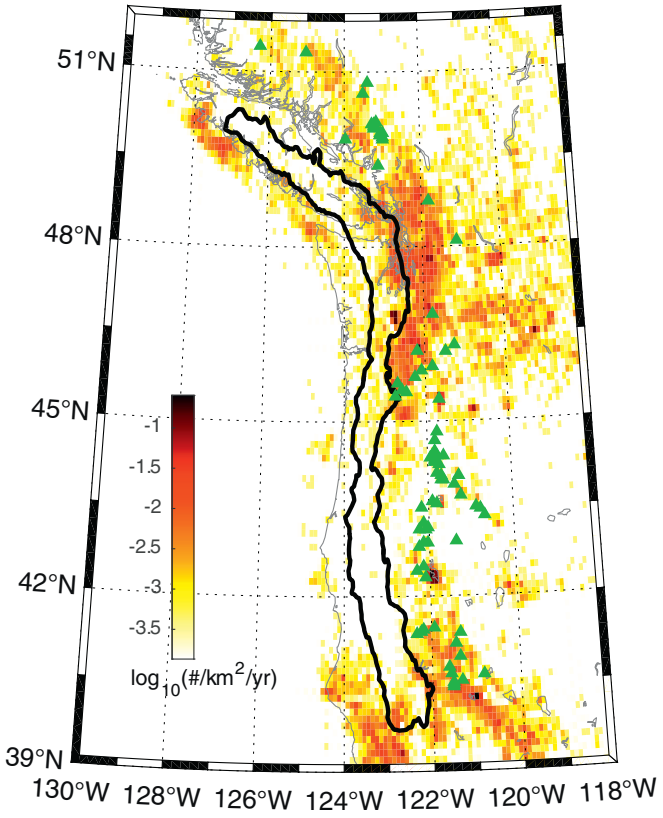

Fig. 3. North America crustal seismicity density (base 10 logarithm of number of events per square kilometer per year) along the Cascadia margin. Green triangles represent locations of volcanic centers.

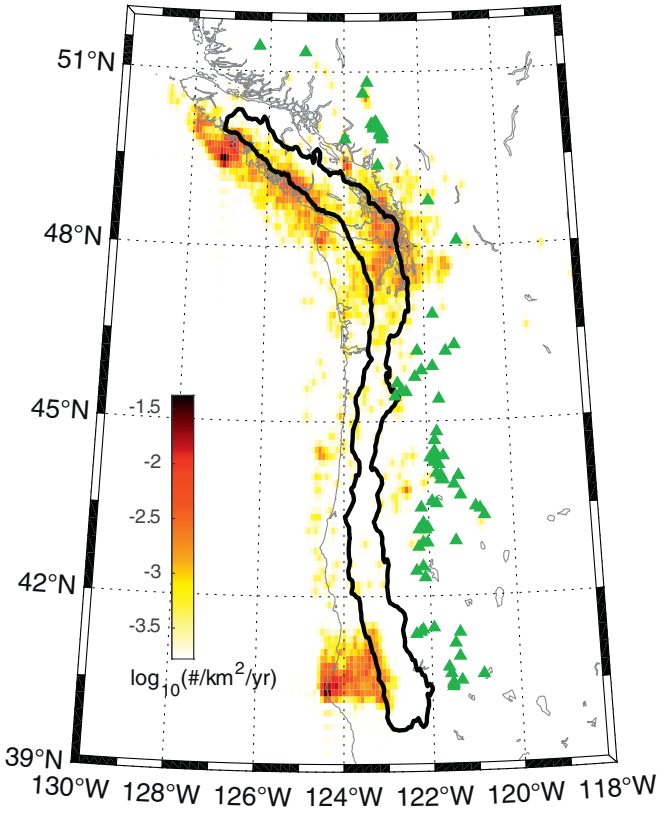

Fig. 4. Juan de Fuca (slab) seismicity density (base 10 logarithm of number of events per square kilometer per year) along the Cascadia margin. Green triangles represent locations of volcanic centers.

(McCrory et al., 2012). In particular there is a narrow strip of shallow (≤40 km) seismicity extending landward to the up-dip limit of tremor between latitudes 40.2–41.5°N. We note that intraslab events are generally characterized by very low levels of aftershock activity (e.g., Kao et al., 2008) such that most of the seismicity represented in Fig. 4 consists of temporally isolated events.

3. Controls on seismicity

In the previous section, we summarized a number of suggestive and previously documented patterns in seismicity along the Cascadia forearc. In particular, we noted i) a slowly meandering band of tremor along the entire subduction margin, ii) a concentration of deep (>40 km) slab seismicity to the Puget Sound region, iii) a concentration of shallow slab seismicity (≤40 km) along western Vancouver Island and northern California, iv) a distribution of crustal seismicity that displays landward concentrations in the Puget lowlands and northern California, and v) a distinct tendency toward anticorrelation in the epicentral distributions of tremor and crustal seismicity, where the latter occurs. In this section we examine several factors that likely play significant roles in defining these patterns, paying particular attention to deviatoric stress (slab pull), strain (slab curvature), metamorphic reactions, and a plate boundary seal whose spatial extent includes that of tremor. This latter element has received rather less attention than the others but we will argue that it plays an important role in the generation of both tremor and crustal seismicity.

3.1. Slab deviatoric stress and tomographic constraints

We begin our analysis by considering deep intraslab seismicity. A number of authors have investigated slab stresses through consideration of focal mechanism solutions. In the Puget Sound region it has long been recognized that deep slab earthquakes tend to be associated with normal faulting focal mechanisms with down-dip directed tension axes (e.g., Crosson, 1981; Rogers, 1983; Spence, 1989). A comprehensive margin-wide study of slab stress by Wada et al. (2010) using deep events revealed the same pattern of down-dip tension for slab events in southern British Columbia, Washington and northern California that they interpreted as the result of slab pull, as others before them (e.g., Spence, 1989). Downdip tension is consistent with deviatoric slab stresses controlled by by negative buoyancy of the deeper subducting plate (Frohlich, 1989). Increased slab density due to cooler temperatures is manifest within teleseismic tomography models as positive velocity anomalies (Audet et al., 2008; Burdick et al., 2017; Obrebski et al., 2010). These models reveal prominent P-velocity anomalies to ≥300 km depth beneath southern BC, Washington and northern California where intraslab earthquakes occur but a conspicuous absence thereof below Oregon (see Fig. 5) where intraslab events are effectively absent, rendering slab pull an obvious potential control on seismogenesis.

3.2. Slab strain from minimum slab curvature

We proceed to examine the potential role of slab strain in influencing slab seismicity by constructing a minimum curvature model of depth to top of the subducting plate (hereafter "slab depth"). Our intention is not to capture the finer details of slab morphology but rather to focus on its long-wavelength structure and, in particular, those regions where extended areas of greater slab strain are expected; actual slab deformation can only be more severe.

In the first step of the model construction, we consider 4 slab depth proxies, sampled evenly and with uniform certainty along strike. The proxies are (see Fig. 6a): the location of the deformation front, the upper and lower limits of tremor from Wech (2010) as depicted in Figs. 3 and 4, and the distribution of the 18 major volcanic centers along the arc. We define the deformation front to represent a slab depth of 2.5 km below msl upon consideration of average bathymetry.

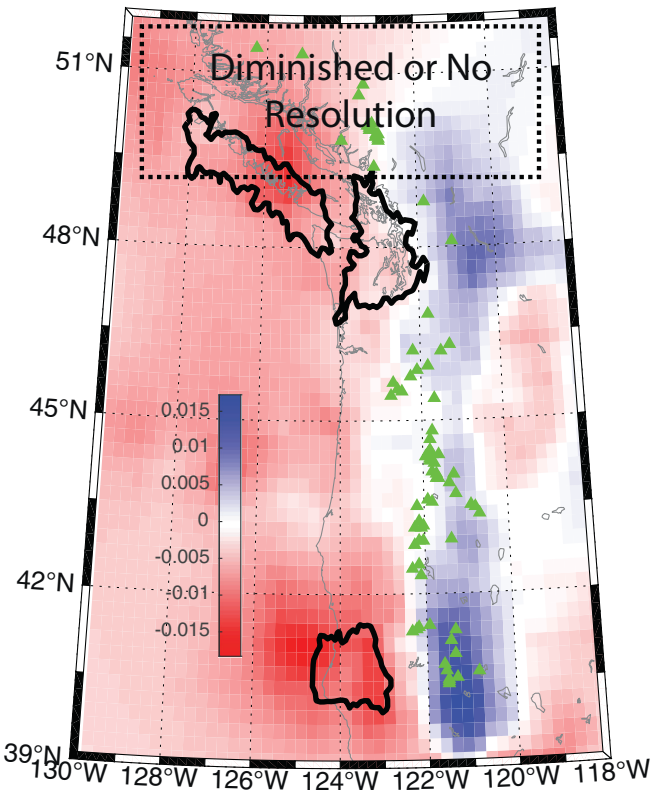

Fig. 5. P-velocity perturbation relative to background (red = slow, blue = fast) at 200 km depth Cascadia margin (Burdick et al., 2017). Outlines of slab seismicity concentrations from Fig. 4 are shown in black. Note that resolution deteriorates in British Columbia north of 49°N due to station coverage in this image but that a NW-trending high-velocity perturbation continues into this region in the model of Audet et al., 2008, their Fig. 3).

Based on studies of LFEs in southern Vancouver Island, Washington (Royer and Bostock, 2014), central Oregon (Thomas and Bostock, 2015) and northern California (Plourde et al., 2015), we assign nominal depths of 28 and 45 km to the up and down dip limits of tremor. This approximation is likely poorest for the Explorer plate in the northern reaches of Cascadia where LFEs align with a nearly horizontal portion of plate boundary between 30 and 35 km depth (Audet et al., 2008; Royer and Bostock, 2014). However, as we shall see, it will prove to be conservative for our purposes. The fourth constraint derives from the volcanic arc where the slab is assigned a nominal depth of 80 km based on scattered wave images of the subducting oceanic Moho (Mann et al., 2017; McGary et al., 2014; Nicholson et al., 2005; Rondenay et al., 2001). In so doing, we assume that variability in the surface distribution of volcanic centers is due to random perturbations about this depth contour resulting from lateral, near-surface deviations in magmatic ascent paths (e.g., Hansen et al., 2016; Bedrosian et al., 2018.). We treat each of these sets of control points in a consistent fashion by converting to Universal Transverse Mercator coordinates and fitting a polynomial of degree 6 to the longitudinal coordinate as a function of the latitudinal coordinate. The resulting slab-depth contours are plotted in black lines above corresponding control points in Fig. 6a.

The low-order polynomial representation provides a faithful description of the deformation front and captures the long wavelength variability in the up- and down-dip limits of tremor. As expected, the modeled depth of arc magma generation exhibits the greatest variance with its (volcanic center) control points. It is notable, however, that its polynomial parameterization closely parallels that of the deformation front along the entire margin. In contrast, the tremor depth curves wind gently between the deformation front and arc-depth contours,

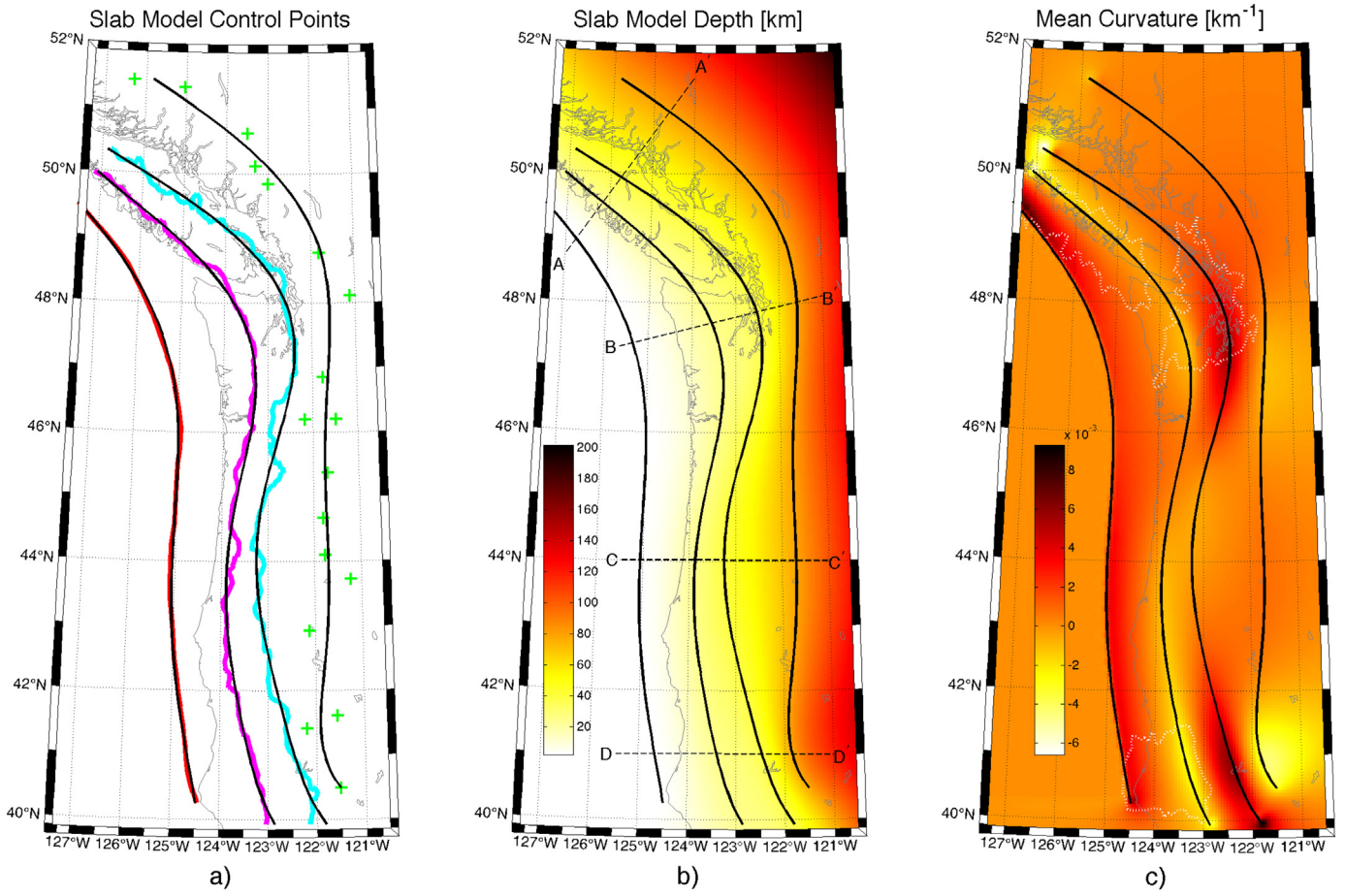

Fig. 6. Long-wavelength slab model. Panel a) shows control points used to construct model: deformation front (red), updip limit of tremor (magenta), downdip limit of tremor (cyan), and major volcanic centers (green plusses). Superposed black lines show corresponding 6th order polynomial parametrizations defining 2.5 km, 28 km, 45 km and 85 km depth contours. Panel b) displays 2D slab model constructed through biharmonic interpolation of these depth contours and locations of profiles in Fig. 7. Panel c) shows curvature of corresponding slab surface. Outlines of slab seismicity concentrations are shown in stippled white.

approaching the arc-depth contour in the Puget Sound and northern California regions and receding from that contour in Oregon. We note that this contour fluctuation is effectively absent in the recent McCrory et al. (2012) slab model (based on a range of slab depth proxies) but is represented within the Audet et al. (2010) model that is based on a coarsely sampled but uniform suite of receiver function depth estimates. This latter correspondence with an independent proxy lends justification to our use of tremor limits as slab depth contours.

In the second step of model construction, we employ the 1-D polynomial parameterizations within a 2-D bi-harmonic spline interpolation to produce a continuous, minimum curvature depth model for the Juan de Fuca slab in Fig. 6b. This simple representation in turn allows us to compute stable estimates of surface curvature (i.e., mean of 2 principal curvatures) plotted in Fig. 6c. Although the synthetic model is not supported by the same density of control points along dip as that of the recent McCrory et al. (2012) model, it holds the advantage that it is uniformly and consistently sampled along strike by the same 4 contour parameters. In contrast, the McCrory et al. (2012) employs geographically variable proxies for slab depth including hypocenter data sets with varying levels of hypocentral precision and a range of structural models based on different geophysical observables.

A correspondence exists between regions of high curvature (i.e. ≥ 0.004 km^{-1}; positive = concave down) and concentrations of slab seismicity. To aid in visualizing variations in slab morphology, we plot profiles across the synthetic model for central Vancouver Island (A-A': red), Puget Sound (B-B′: blue), central Oregon (C-C′:green) and northern California (D-D' (magenta) in Fig. 7 with locations marked in Fig. 6b. We note in particular, the broad, shallow dipping arch (Rogers, 1983; Weaver and Baker, 1988) defined by the tremor contours below Puget Sound followed down-dip by high slab curvature in the vicinity of where the largest slab events in Cascadia (e.g., Kao et al., 2008) are recorded. High model curvature in this region is strongest in the dip direction and generated by the proximity of the down-dip tremor contour with that of the volcanic arc resulting in a steep increase in slab dip. In

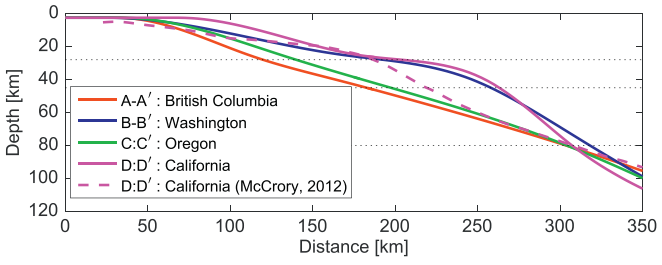

Fig. 7. Profiles across synthetic slab model at the 4 locations shown in Fig. 6b. Note strong curvature at slab depths near 40 km across Washington (solid blue) and northern California (solid magneta), with minor or little changes in slope across central Vancouver Island (solid red) and Oregon (solid green). The dashed magenta line represents the plate model of McCrory et al. (2012) which is precisely defined by double difference relocated hypocenters (Fig. 8) at top-of-slab depths <30 km but is unconstrained below. A composite plate model that stitches the latter model to the synthetic (solid magenta) curve at depths ≥30 km would better accommodate constraints from tremor (Plourde et al., 2015) and imply a steeper slab dip toward the arc.

contrast, as one moves to the northwest, the tremor contours shift their course and approach the deformation front, creating greater curvature in the model offshore Vancouver Island in rough correspondence with the location of shallow slab events documented for that region (Rogers, 1983; Wada et al., 2010). This spatial coincidence suggests tensional stresses due to shallow slab flexure as a possible alternative mechanism to that of a torque force on the Nootka fault zone proposed by Wada et al. (2010) to explain dip-parallel tension axes for these events. Slab curvature would be greater still were we to have assigned a more accurate range of slab depths to the tremor contour in this region (30–35 km vs 28–45 km). In fact, a depth profile of seismicity near the Nootka Fault Zone that includes LFE hypocenters (Gao and Wang, 2014; Royer and Bostock, 2014) strongly suggests that actual slab structure exhibits a strong bend at shallow depths just seaward of the deformation front (see Fig. 8 and location of profile in Fig. 1) coinciding with a marked increase in seismicity and a landward flattening of the slab (Audet et al., 2010). We further note that slab curvature in Fig. 6c is preferentially oriented in the dip (versus strike) direction and hence would be expected to generate down-dip tension axes in slab earthquake focal mechanisms occurring above the mid-plane of the slab. Thus slab curvature also affords an alternative explanation to slab pull for deep slab events beneath Puget Sound. In fact, it is conceivable that slab curvature is influenced by slab pull, at least at depths near 40 km, though we consider them separately for the present purpose.

The correspondence between model curvature and slab seismicity is not, however, evident in northern California. Convergent tremor and arc contours again predict a region of high slab curvature below the down-dip limit of tremor that is without a slab seismicity counterpart. Slab seismicity is instead effectively limited to depths ≤40 km and restricted to parts effectively seaward of the up-dip tremor limit. McCrory et al. (2012) have demonstrated that the top of slab in this region is concave positive from the deformation front to approximately 20 km depth, whereupon it becomes concave negative at 25 km depth before reversing again to become concave positive at greater depths (see Figs. 7, 8). This bending/unbending takes place over a greater strike-perpendicular distance than that at the Nootka Fault Zone (~150 vs ~60 km) but nonetheless occurs inside the limits represented by the model deformation front and up-dip tremor-limit contours in Figs. 6, 7 and so is, naturally, absent within our minimum curvature slab-depth model. However, it is captured within the McCrory et al. (2012) slab model that is entirely constrained in this region by double-difference relocated hypocenters (Figs. 7, 8). The fact that significant plate bending occurs at shallow depths at both ends of the Cascadia subduction zone (Nootka Fault Zone and Mendocino Triple Junction, Fig. 8) suggests that plate-edge interactions play a significant role in plate deformation and, hence, seismicity in those regions.

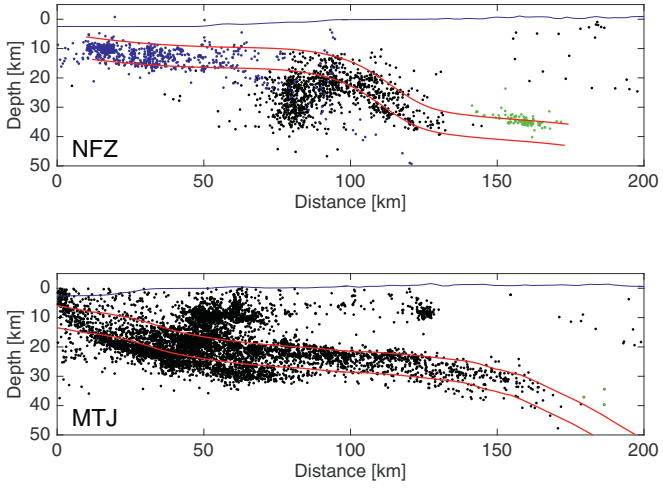

Fig. 8. Seismicity and plate bending/unbending at the northern (top panel) and southern (bottom panel) termini of Cascadia subduction. Top panel shows strike-perpendicular section of seismicity near Nootka Fault Zone (NFZ, dotted red profile in Fig. 1) assembled from the SeaJade OBS experiment (blue dots, Obana et al., 2014), and relocated regular seismicity (black dots) and LFEs (green dots) from Savard (2018). Blue line displays bathymetry/topography with respect to mean sea level, whereas red line is interpreted oceanic crust. Bottom panel shows strike-perpendicular section of relocated seismicity (black dots) immediately north of Mendocino Triple Junction (MTJ, dotted magenta profile in Fig. 2) with superposed slab model (red) from McCrory et al. (2012), and 3 LFEs (green dots) from Plourde et al. (2015). Note different scales of plate bending/unbending at opposing ends of the subduction zone. Concentration of crustal seismicity near MTJ at 10 km depth, 55 km distance represents a temporally persistent cluster of seismicity that includes the 1992 M7.1 Cape Mendocino earthquake and its aftershocks (McCrory et al., 2012).

Consequently, although focal mechanisms and tomographic models implicate some combination of slab curvature and slab pull in the generation of deviatoric stresses that contribute to seismogenesis within the slab, there is sufficient along-strike variability in where slab seismicity occurs to implicate other contributing factors. A point worth noting, however, is that the distribution of crustal seismicity in the deep crustal forearc regions of Puget Sound and northern California displays a significantly stronger correspondence with slab curvature. Crustal seismicity neatly parallels the high curvature regions in the model (compare Fig. 3 with Fig. 6c), although as mentioned it is shifted slightly landward, immediately down-dip of the down-dip tremor contour. We will return to this observation in section 3.5.

3.3. Metamorphic dehydration reactions

Metamorphic reactions taking place within the subducting slab due to increased temperatures and pressures have long been implicated in the generation of intermediate depth seismicity and, in recent years, much attention has been directed toward dehydration reactions in this regard (e.g., Hacker et al., 2003; Peacock and Wang, 1999; Rogers, 1983). Water enters the oceanic crust and mantle primarily through hydrothermal circulation at the ocean ridges and again, just prior to subduction, along normal faults generated through slab flexure at the outer rise (e.g., Peacock, 2001). At low temperatures, water is stored largely in solid form within hydrous minerals and in open cracks and pores. As Cascadia represents a warm end member across subduction zones, much of this water is released as free fluid by dehydration reactions occurring at relatively shallow depths below the forearc (Peacock, 2009; Peacock and Wang, 1999). Rogers (1983) was among the first studies to argue that slab earthquakes in the Puget Sound arch region are enabled by stresses induced through volume reduction accompanying eclogitization of oceanic crust. He further noted that these volume reductions were approximately commensurate with the excess slab volumes created by shallow subduction of the Juan de Fuca plate below the concave-seaward deformation front.

Although other mechanisms (shear heating etc) have been proposed, dehydration embrittlement is at present the most widely cited explanation for intermediate depth seismicity with the two leading candidate reactions being eclogitization of oceanic crust (e.g., Hacker, 1996) and the dehydration of serpentinized (antigorite) oceanic mantle (e.g., Peacock, 2001; Ulmer and Trommsdorff, 1995). The fluids released in these reactions are thought to increase pore pressures, reduce effective stress and promote brittle failure. Earlier studies that identified deep slab seismicity in northern Cascadia as residing primarily within subducting oceanic crust (Cassidy and Ellis, 1993; Hyndman et al., 1990) have been superseded by research placing some (Cassidy and Waldhauser, 2003; Preston et al., 2003) to most slab seismicity within the uppermost mantle (Abers et al., 2013; Bostock, 2013), due in large part to the recognition of a significant (>5 km) depth separation between LFEs and regular slab earthquakes. Moreover, shallow slab earthquakes off the coast of Vancouver Island and at the Mendocino triple junction occur at depths too shallow to be the result of eclogitization.

Thus to the degree that dehydration reactions play a role in the generation of intraslab earthquakes, antigorite dehydration is implied for

much if not most slab seismicity. Dehydration of antigorite occurs at temperatures of 650–700 °C and is largely independent of pressure (for $P < 3$ GPa) (Ulmer and Trommsdorff, 1995). Hence this reaction is expected to occur in subducting mantle at shallow depths in warm subduction zones such as Cascadia. Thermal modelling (e.g., Gao et al., 2017; Gao and Wang, 2014) for northern Cascadia is broadly consistent with shallower depths of antigorite dehydration off northern Vancouver Island than more southerly regions (e.g., Puget Sound), though the variations in seismicity patterns along strike are less regular than would be anticipated were this metamorphic reaction the primary agent of seismicity. Hence, it appears likely that slab seismicity is governed by an interplay between metamorphic dehydration reactions and variable stresses due to slab structure and geometry (McCrory et al., 2012). The influence of metamorphic dehydration likely extends beyond slab seismicity in creating conditions conducive to both the generation of tremor and crustal seismicity. This role centers on fluid production within the oceanic crust and its subsequent evolution. Further insight into this evolution can be gleaned from analysis of tremor and LFEs.

3.4. Plate boundary seal

As discussed in section 2.1, LFE hypocenters are mapped to a narrow depth range in Cascadia and LFE waveform polarizations are consistent with thrust motion on a shallow dipping plane. Moreover, LFE hypocenters also coincide with a thin layer of strongly depressed shear velocity, elevated Poisson's ratio (e.g., Audet et al., 2009; Cassidy and Ellis, 1993), and high seismic reflectivity and high conductivity (e.g., Hyndman, 1988) that we interpret as overpressured upper oceanic crust (Christensen, 1984; Hansen et al., 2012). The various geophysical measurements lead to estimates of free fluid content of approximately 3% (Hyndman, 1988; Peacock et al., 2011). The close association between LFEs and this pronounced low velocity zone (LVZ) together with a well-documented sensitivity of tremor/LFEs to minor stress perturbations (e.g., Houston, 2015; Royer et al., 2014; Rubinstein et al., 2009) indicates that tremor is generated within a persistently overpressured environment in which effective stresses are very low. This observation is consistent with the expectation that fluids generated through metamorphism are produced at lithostatic pore pressure. Under the assumption that porosity within oceanic crust is dominated by interconnected cracks, the maintenance of overpressures also requires the presence of an impermeable seal at the top of the LVZ (Peacock et al., 2011). This seal effectively prevents fluid transfer from the subducting slab into the overriding plate or mantle wedge over, and potentially beyond, the range where tremor is documented. It may form through deformation-induced grainsize reduction and the development of highly foliated cataclasites and mylonites (Angiboust et al., 2015; Peacock et al., 2011).

This line of reasoning provides motivation for a “pore-pressure-threshold” model to describe the generation of tremor. That is, as metamorphic dehydration reactions proceed, fluid pressures build owing to the presence of the plate boundary seal and eventually reach a threshold level at which tremor and low frequency earthquakes are generated. The underlying physics may involve reductions in Coulomb strength, changes in rate and state frictional parameters or both, through their dependencies on effective stress (Scholz, 2002). The threshold model is consistent with the observation that Cascadia tremor density is muted below major crustal faults implying that such faults provide fracture pathways for fluid escape from and pore-pressure reduction within subducting oceanic crust (Wells et al., 2017). Development of the plate boundary seal and overpressures likely commences offshore, based on marine seismic reflection studies (Bostock, 2013; Nedimovic et al., 2003) and OBS receiver function analyses (Audet and Schaeffer, 2018; Janiszewski and Abers, 2015) but threshold pore pressures are not met until the slab has reached depths near 28 km, the nominal up-dip limit of tremor, below the continental forearc. It is conceivable that higher pore pressures are required for tremor generation than for the occurrence of slow slip that is documented to occur farther up dip than tremor in the southern Vancouver Island region (e.g., Dragert and Wang, 2011).

The processes that lead to down-dip termination of tremor may involve a drop in pore pressure or a change in plate boundary rheology. It is notable, however, that the strong parallelism in up- and down-dip tremor contours, their transitions and general consistency in LFE depths along the margin suggests similar sensitivities to physical properties, e.g., pressure and temperature. Another constraint arises from the observation that the down-dip tremor limit appears to coincide with an abrupt reduction in the contrast of the LVZ as imaged in receiver function images across southern Vancouver Island, southern Puget Sound and central Oregon (Abers et al., 2009; Bostock et al., 2002; Nicholson et al., 2005). This termination is generally interpreted to indicate the onset of eclogitization, consistent with thermal and petrologic modelling at shallow depths near 45 km in Cascadia (Peacock and Wang, 1999; Rondenay et al., 2008). Thermal-petrological modelling by Abers et al. (2013) suggests that transformation of metabasalt to eclogite along warm subduction zone P-T paths is exothermic with a net volume reduction between total reactant and product mineralogies, including solid and fluid phases, across the multi-component phase boundary. In the context of the pore-pressure threshold model outlined above, it is conceivable that the volume decrease associated with this reaction could cause pore pressures to decrease below the tremor threshold, resulting in the cessation of tremor. Accordingly, the down-dip limit of tremor in this interpretation represents a proxy for the onset of oceanic crustal eclogitization. Previous authors (Audet et al., 2009; Savard et al., 2018) have further proposed that eclogitization compromises the plate boundary seal enabling fluids to escape the slab. The mechanism through which the breach is achieved is unclear, however, and one might reasonably expect the seal to persist after pore pressures drop. We will return to this point in the following section.

3.5. Fluid escape

A number of observations indicate that fluids generated through dehydration reactions within the subducting slab in Cascadia eventually escape into the overriding forearc mantle wedge and continental crust. Hydration of the mantle wedge (Hyndman and Peacock, 2003; Peacock, 1993) has been proposed by several authors based on the observation of a weak, absent or inverted continental Moho along most of the forearc that is inferred to be due to the juxtaposition of continental crust with an extensively serpentinized mantle wedge (Bostock et al., 2002; Brocher et al., 2003; Hansen et al., 2016). The timing of mantle wedge serpentinization is not well constrained given the extended history (≥40 Ma) of subduction along the margin, and relative thermal stability of a serpentinized wedge (cf. Kirby et al., 2014). Helium (He^3/He^4) ratios that measure the proportion of primordial to radiogenic helium provide evidence that slab fluids eventually find their way into the continental crust. McCrory et al. (2016) have measured He^3/He^4 in mountain springs along the margin and documented a punctuated increase in He^3/He^4 proceeding landward into the forearc region suggesting a focused expulsion of fluids beginning above the mantle wedge corner.

Additional evidence for ingress of slab fluids into the continental crust arises in traveltime inversion studies of crustal structure beneath southern Vancouver Island and environs that indicate the presence of low Poisson's ratio anomalies in the forearc crust above the mantle wedge. Ramachandran and Hyndman (2012) and Hyndman et al. (2015) attributed these features to silica precipitation from slab fluids originating in the slab. Their model involves slab fluids directed into a cool forearc crust immediately seaward of the wedge corner by the presence of a serpentinized and impermeable wedge mantle. Using an expanded traveltime data set, Savard et al. (2018) have imaged the same region with double-difference tomography (Zhang and Thurber, 2003) and noted an association between low Poisson's ratio regions

and elevated levels of clustered seismicity down-dip of tremor, consistent with Fig. 3. They proposed that significant quantities of quartz within the forearc crust are produced through metasomatic reactions enabled by fluids fluxed through the mantle wedge down-dip of the plate boundary seal. This explanation obviates mass balance issues that arise with the slab-silica precipitation hypothesis. These same fluids are inferred to promote increased levels of clustered seismicity within the continental crust through fault-valve seismic pumping (Sibson et al., 1988). Accordingly, we consider clustered seismicity in the Cascadia forearc crust to represent an additional proxy for the ingress of slab fluids (cf., Vidale and Shearer, 2006).

We now return to the variable spatial distribution of forearc crustal seismicity and its correlation with regions of large-scale slab curvature. As discussed in section 2.2 and evident in Fig. 3, high concentrations of crustal seismicity are sandwiched between the down-dip limit of tremor and the volcanic arc in the Puget Sound region and northern California. In the context of the pore-pressure threshold model, the general paucity of crustal seismicity in the tremor epicentral region is simply explained by the presence of the plate boundary seal and a consequent lack of high fluid concentrations through most of the overlying crust. However, the appearance of crustal seismicity and other fluid proxies immediately landward of tremor epicenters implies that fluids escape from the slab beneath the mantle wedge in these two regions but are prevented from doing so in adjacent locations along strike, i.e. Oregon and British Columbia, where forearc crustal seismicity is largely absent.

An explanation for this along-strike variability in crustal seismicity is supplied by the long wavelength slab structure presented in Figs. 6, 7. Puget Sound and northern California represent regions of high, positive, slab curvature below the landward forearc that closely mirror the along-strike distribution of seismicity concentrations landward of the tremor zone. Conversely, the large separations between tremor and volcanic arc (and more specifically, the inferred slab isodepth contours) in Oregon and north/central Vancouver Island imply a more gradual and subdued bend in the subducting slab (Fig. 7). The spatial correspondence between model slab curvature and crustal seismicity implies that fluid expulsion from the slab into the forearc is further controlled by slab curvature. Tensional stresses due to positive (concave down) slab curvature are greatest at the top of the slab and we posit that resulting extensional strains breach the plate boundary seal and release fluids from the subducted oceanic crust into the forearc crust beneath Puget Sound and northern California promoting seismicity. Beneath Oregon and north/central Vancouver Island, we propose that tensional stresses are insufficient to compromise the seal at these levels, forcing fluids to greater depths prior to their release below the volcanic arc.

4. Implications

In the previous section we proposed that spatial patterns in the distribution of seismicity in Cascadia are governed by the interplay between 3 essential factors: deviatoric stresses due to slab pull/curvature, pressure- and temperature-dependent metamorphic reactions, and the development and compromise of a plate boundary seal which controls where fluids exit the slab. We now proceed to examine the broader implications of these inferences.

4.1. Mantle wedge hydrology

One of the primary motivations for the fluid-evolution model detailed in section 3.5 arises from the previously documented anticorrelation in epicentral distributions of tremor and crustal seismicity, in particular where the latter occurs landward of tremor in southwestern British Columbia, Washington and northern California (Fig. 3, Kao et al., 2009; Boyarko and Brudzinski, 2010). The boundary between these two distributions, namely the down-dip limit of tremor, must generally coincide with slab depths close to our nominal 45 km value, based on hypocentral locations of the deepest LFEs. The model thus implies that fluids fluxed from the slab down-dip of tremor must traverse ~10 km or more of substantially serpentinized mantle (e.g., Nicholson et al., 2005). The inferred causality between high slab curvature and crustal seismicity concentrations further implies a fluid flux from slab through to crust that is steady state at time scales <<1 Ma. An alternate interpretation whereby fluids originate within a dehydrating wedge (i.e. serpentinized at some earlier time) as a result of, for example, secular warming of the incoming subducting plate (cf. Kirby et al., 2014), fails to account for this association. Vidale et al. (2014) have suggested that deep long-period earthquakes (or DLPs) observed within the forearc mantle wedge at depths of 36–45 km in central Oregon (with low levels of crustal seismicity, Fig. 3) may manifest embrittlement created through antigorite dehydration, a scenario that our model will accommodate. That is, lower levels of forearc crustal seismicity in Oregon may result from commensurately lower fluid fluxes sourced from a dehydrating wedge with little or no present-day contribution from the slab. The higher density of regular earthquakes in the crust overlying forearc DLPs in central Oregon lends some support to this conjecture (see Vidale et al., 2014, their Fig. 4). We note, however, that DLPs originating in the mantle wedge have yet to be detected outside of Oregon.

A long-standing debate (e.g., Moody, 1976; O'Hanley, 1992) has existed concerning whether serpentinization proceeds under constant composition or constant volume conditions. Serpentinization of peridotite at constant composition (i.e. closed system after addition of water) leads to major increases in volume of 30–50%. Much attention in recent years has focused on understanding permeability development during serpentinization (e.g., Malvoisin et al., 2017; Rudge et al., 2010). Our association of crustal seismicity with regions of high tensional strain at the slab surface would suggest that permeability development within the mantle wedge is sufficient to maintain significant vertical fluid fluxes over time scales <<1 Ma, nothwithstanding predictions of low-permeability, sheared serpentinite above the slab interface (Katayama et al., 2011). The potential field signature of wedge serpentinization involves coincident negative gravity and positive magnetic anomalies that extend along a margin-parallel strip of the Cascadia forearc (Blakely et al., 2005). This combination is unusual among common crustal lithologies but consistent with presence of low-density (~2.6 g/cm^3) antigorite and magnetite generated as a by-product of serpentinization of the mantle wedge (Evans, 2008). The potential field anomaly also coincides with the Puget Sound/Willamette Valley lowlands, thus challenging the notion that serpentinization should give rise to topographic highs as a result of volume increase (Fyfe and McBirney, 1975). Resolution of this conundrum will likely require combined thermo-mechanical, petrological and fluid dynamical modelling accounting for fluid production, consumption and migration accompanying mantle serpentinization and crustal eclogitization.

4.2. Forearc crust

It is conceivable that fluid escape into the forearc crust down-dip of tremor is sustained over geologic time scales (≥10 Ma) commensurate with the duration of “warm subduction” conditions, and thereafter through dehydration of a relict mantle wedge (Kirby et al., 2014). The forearc crust in such instances may be considered as extreme among terrestrial environments as regards prolonged exposure to fluid flow, an inference with relevance to crustal composition. Several authors have noted low Poisson's ratio anomalies in forearc (e.g., Doi et al., 2013; Halpaap et al., 2018; Hyndman et al., 2015; Kato et al., 2010; Ramachandran and Hyndman, 2012; Savard et al., 2018) and former forearc crust (Lin and Shearer, 2009), often in association with clustered seismicity and inferred fluids. Explanations typically involve either the presence of excess (alpha-) quartz that has an unusually low Poisson's ratio (e.g., Christensen, 1996) or the presence of fluid filled porosity with more equant geometry (e.g., Takei, 2002). Metasomatic reactions within forearc crust enabled by fluids fluxed from the slab may allow

both mechanisms to play a role in the generation of these anomalies. Many of these reactions produce quartz at the expense of other silica bearing minerals via cation replacement and involve net solid volume reduction (e.g., Savard et al., 2018). Evidence for in-situ quartz generation within forearc crust has been reported by Fisher et al. (1995), and support for porosity development through fluid induced metasomatic alteration associated with earthquake swarms and low Poisson's ratios (Dahm and Fischer, 2014), is presented by Heinicke et al. (2009) for low pH systems.

An association between quartz, fluids and swarm seismicity is also noted in the context of orogenic ("meso-thermal") gold deposits (Cox, 2016; Sibson et al., 1988) begging the question as to whether a genetic link exists with warm subduction zone environments (Savard et al., 2018). Goldfarb and Groves (2015) argue that such deposits can be formed through fluids fluxed into the forearc crust from a devolatilizing slab or mantle wedge. It is tempting to further speculate as to whether the substantial representation of orogenic gold deposits formed in the late Archean (e.g., Cawood and Hawkesworth, 2013) results from a greater prevalence of warm subduction earlier in Earth's history. It is worth remarking that southern Vancouver Island has a history of gold mining with initial discovery in the Leech River in 1864. This river formed above the Leech River Fault, a major structural feature marked by clustered microseismicity (Li et al., 2018; Morell et al., 2017; Savard et al., 2018), which transects an extensive low Poisson's ratio anomaly in the Cascadia forearc crust (Savard et al., 2018).

4.3. Volcanism

The locations where fluids produced by metamorphic dehydration reactions exit the slab are expected to influence the general patterns of arc volcanism. Dehydration in warm subduction zones, such as Cascadia, involving the subduction of young oceanic plates is anticipated to initiate at shallow depths such that any fluids lost to the forearc are unavailable to promote magma generation (Kirby et al., 1996). Hence, warm subduction zones are frequently cited as having low volcanic output, although Hildreth (2007) provides compelling arguments that Cascadia volcanic output in the Quaternary is not low relative to other arcs (e.g., NE Japan, central America, Alaska Peninsula), in particular through Oregon. Sherrod and Smith (1990) estimated extrusion rates along the Cascade arc within the past 2 Ma. They noted high extrusion rates (3–6 km^3/km/Ma) in central Oregon, flanked by lower rates in southern Washington (1.6 km^3/km/Ma) and northern California (3.2 km^3/km/Ma), with the lowest rates in northern Washington and British Columbia (0.21 km^3/km/Ma). Accounting for preservation bias due to glaciation does not affect this hierarchy in extrusion rates (Hildreth, 2007). Consequently, there is general anticorrelation between concentrations of seismicity and volcanic output. Following from section 3.5, it is natural therefore to propose that increased slab curvature enables fluid escape at shallower slab depths leading to higher levels of forearc seismicity, whereas smooth slab topography promotes the fluid retention to greater depths (≥ 80 km) and more prodigious melt generation.

The one segment of Cascadia that does not conform to this pattern is the Garibaldi volcanic belt in British Columbia that is characterized by both low levels of volcanic output and low concentrations of forearc seismicity. Along this stretch of arc there are 2 additional variables to consider relative to other portions of the subduction zone. They are the rapid decrease in plate age and a change in stress regime, both influenced by the switch in margin strike from north to northwest. It has been argued that the northward transition to a more compressive state, reduces the penetration of magmas into and through the crustal column (Hildreth, 2007; Rogers, 1985). Low levels of crustal seismicity persist to the northwest in British Columbia in Fig. 3, but appear to be focussed below the arc as opposed to the intervening forearc downdip of tremor. It is conceivable that these events are related to magmatic processes.

We note that previous authors have linked slab morphology with volcanic output. Guffanti and Weaver (1988) divided the Cascade arc into segments that relate to inferred changes in geometry of the subducting Juan de Fuca plate as defined by slab seismicity in the Puget Sound and northern California. They specifically identified the influence of the Puget Sound arch (Weaver and Baker, 1988) and defined segment boundaries in northern Oregon and northern California that roughly delimit the region of shallow slab curvature shown in Fig. 6. Our results can thus be considered a refinement of this earlier work.

4.4. Other subduction zones

The factors identified in section 3 as controlling seismicity in Cascadia should be demonstratively operative in other warm subduction zones to have general validity. The influence of slab pull/geometry (e.g., Frohlich, 1989; Spence, 1987) and metamorphic dehydration reactions (e.g., Hacker et al., 2003; Peacock and Wang, 1999) have been long and extensively considered in the context of slab seismicity. Here we will focus instead on the proposed significance of a plate boundary seal, which has not hitherto received widespread attention. The least ambiguous proxy for the presence of the plate boundary seal is the documentation of tectonic tremor that, in the range of environments it has been observed to date, bears an association with near-lithostatic fluid pressures. Tectonic tremor is most prominently expressed in warm subduction zones (Ide, 2012). Here we consider two subduction zones with tectonic tremor comparable to that in Cascadia, namely eastern Alaska and southwest Japan.

Tremor was initially identified in eastern Alaska by Peterson and Christensen (2009) and an extensive tremor catalog has since been assembled by Wech (2016) who mapped a broad tremor region extending over 500 km along strike. Chuang et al. (2017) extracted a suite of LFE templates from tremor to constrain their depths. Tremor/LFEs in Alaska extend over a similar along-dip width (between 40 and 80 km) to Cascadia but occur down-dip of the mantle wedge (as opposed to straddling it) between 40 and 60 km depth. These authors also documented (see their Fig. 2a) an anticorrelation between epicenters of tremor and regular earthquakes, and a marked increase in crustal seismicity immediately landward of the down-dip limit of tremor, like that in Cascadia. Moreover, they explained the absence of volcanism down-dip of tremor (the Denali volcanic gap, see Rondenay et al., 2010) as due to shallow release of slab fluids from the uppermost crust of the subducted Yakutat plateau. These correlations between tremor, seismicity and volcanism are consistent with the fluid evolution model we have outlined above for Cascadia.

Tremor zone width in Nankai, averaging near 20 km, is significantly narrower than that in Cascadia and its trajectory winds more widely, implying significant contortions in plate geometry (Obara, 2002). This narrow width renders it more difficult to assess an anticorrelation with crustal seismicity since some lateral diffusion of fluids is expected upon migration to the surface, thereby blurring epicentral distributions. Nakajima and Hasegawa (2016) have examined crustal velocity structure immediately above slab depths at which tremor occurs. These authors observed that tremor activity is anticorrelated with large (positive and negative) excursions in Vp/Vs, negative perturbations in Vp and Vs, and increased attenuation and splitting. They argued that such signatures relate to the increased levels of crustal metamorphism above regions with diminished or absent tremor activity, caused by fluid escape from the slab in these regions. This interpretation is consistent with the observation of reduced tremor density below major crustal faults in Cascadia (Wells et al., 2017), and the notion of a pore-fluid pressure threshold for tremor generation. We further speculate that high levels of both crustal and slab seismicity in the Nankai forearc manifest the interplay of large deviatoric stresses and strains resulting from high levels of slab curvature with metamorphic dehydration in warm slab conditions. In comparison with Cascadia, this combination

of factors results in a more complete expulsion of slab fluids within the Nankai forearc, leading to a near absence in arc volcanism.

5. Conclusions

Much of our analysis of the controls on seismicity patterns in Cascadia draws upon observations and relations that have long been recognized or suspected; notably the importance of slab geometry and metamorphic dehydration. The novel element in our treatment arises in the exploitation of tremor and low frequency earthquakes for the constraints they deliver on i) the distribution of a plate boundary seal that controls fluid retention/expulsion within/from the slab, and ii) and the long-wavelength morphology of the subducting plate along the Cascadia margin as a proxy for slab strain, that together deliver insights into the along-strike variability in forearc crustal seismicity. A simple model of shallow fluid release down-dip of tremor in regions of strong slab curvature provides a cogent explanation for the distribution of concentrated seismicity within the forearc of the North American plate with broader implications. In particular, it affords insight into systematic variations in volcanic extrusion rates along the Cascade arc, hydrological properties of the serpentinized mantle wedge, and compositional modification of the North Amercan forearc crust through metamorphism and metasomatism aided by focused fluid infiltration. These processes are likely to be of general relevance to warm subduction environments elsewhere, in both the past and present day.

Acknowledgments

We are grateful to the associate editor and two reviewers for their constructive criticisms. MB thanks special issue editor Philippe Agard for encouraging this contribution and for the opportunity to engage in wide-ranging discussions concerning subduction processes through the ZIP ITN project. We thank Koichiro Obana for access to SeaJade 1 hypocenters. This research was supported by Natural Sciences and Engineering Research Council of Canada Discovery Grant RGPIN-2016-04239 to MB.

Appendix A. Supplementary data

Supplementary data to this article can be found online at https://doi.org/10.1016/j.lithos.2019.02.019.

References

Abers, G.A., MacKenzie, L.S., Rondenay, S., Zhang, Z., Wech, A.G., Creager, K.C., 2009. Imaging the source region of Cascadia tremor and intermediate-depth earthquakes. Geology 37, 1119–1122. https://doi.org/10.1130/G30143A.1.

Abers, G.A., Nakajima, J., van Keken, P.E., Kita, S., Hacker, B.R., 2013. Thermal-petrological controls on the location of earthquakes within subducting plates. Earth and Planetary Science Letters 369–370, 178–187. https://doi.org/10.1016/j.epsl.2013.03.022.

Adams, J., 1990. Paleoseismicity of the Cascadia subduction zone: evidence from turbidites off the Oregon–Washington margin. Tectonics 9, 569–583.

Angiboust, S., Kirsch, J., Oncken, O., Glodny, J., Monie, P., Rybacki, E., 2015. Probing the transition between seismically coupled and decoupled segments along an ancient subduction interface. Geochemistry, Geophysics, Geosystems 16, 1905–1922. https://doi.org/10.1002/2015GC005776.

Armbruster, J.G., Kim, W.-Y., Rubin, A.M., 2014. Accurate tremor locations from coherent S and P waves. Journal of Geophysical Research 119, 5000–5013. https://doi.org/10.1002/2014JB011133.

Atwater, B.F., 1987. Evidence for great Holocene earthquakes along the outer coast of Washington state. Science 236, 942–944.

Audet, P., Schaeffer, A.J., 2018. Fluid pressure and shear zone development over the loced to slow slip region in Cascadia. Science Advances 4, 2982. https://doi.org/10.1126/sciadv.aar2982 eaar.

Audet, P., Bostock, M.G., Mercier, J.-P., Cassidy, J.F., 2008. Morphology of the Explorer-Juan de Fuca slab edge in northern Cascadia: Imaging plate capture at a ridge-trench-transform triple junction. Geology 36, 895–898. https://doi.org/10.1130/G25356A.1.

Audet, P., Bostock, M.G., Christensen, N.I., Peacock, S.M., 2009. Seismic evidence for overpressured subducted oceanic crust and megathrust fault sealing. Nature 457, 76–78. https://doi.org/10.1038/nature07650.

Audet, P., Bostock, M.G., Boyarko, D.C., Brudzinski, M.R., Allen, R.M., 2010. Slab morphology in the Cascadia fore arc and its relation to episodic tremor and slip. Journal of Geophysical Research 115, B00A16. https://doi.org/10.1029/2008JB006053.

Balfour, N.J., Cassidy, J.F., Dosso, S.E., 2012. Identifying active structures using double-difference earthquake relocations in Southwest British Columbia and the San Juan Islands, Washington. Bulletin of the Seismological Society of America 102, 639–649. https://doi.org/10.1785/0120110056.

Bedrosian, P.A., Peacock, J.R., Bowles-Martinez, E., Schultz, A., Hill, G.J., 2018. Crustal inheritance and a top-down control on arc magmatism at Mount St Helens. Nature Geoscience 11, 865–870. https://doi.org/10.1038/s41561-018-0217-2.

Blakely, R.J., Brocher, T.M., Wells, R.E., 2005. Subduction-zone magnetic anomalies and implications for hydrated forearc mantle. Geology 33, 445–448. https://doi.org/10.1130/G21447.1.

Blakely, R.J., Sherrod, B.L., Weaver, C.S., Wells, R.E., Rohay, A.C., Barnett, E.A., Knepprath, N.E., 2011. Connecting the Yakima fold and thrust belt to active faults in the Puget Lowland, Washington. Journal of Geophysical Research 116, B070105. https://doi.org/10.1029/2010JB008091.

Bostock, M.G., 2013. The Moho in subduction zones. Tectonophysics 609, 547–557. https://doi.org/10.1016/j.tecto.2012.07.007.

Bostock, M.G., Hyndman, R.D., Rondenay, S., Peacock, S.M., 2002. An inverted continental Moho and serpentinization of the forearc mantle. Nature 417, 536–538. https://doi.org/10.1038/417536a.

Botev, Z.I., Grotowski, J.F., Kroese, D.P., 2010. Kernel density estimation via diffusion. The Annals of Statistics 38, 2916–2957. https://doi.org/10.1214/10-AOS799.

Boyarko, D.C., Brudzinski, M.R., 2010. Spatial and temporal pattners of non-volcanic tremor along the southern Cascadia subduction zone. Journal of Geophysical Research 115, B00A22. https://doi.org/10.1029/2008JB006064.

Brocher, T.M., Parson, T., Trehu, A.M., Snelson, C.M., Fischer, M.A., 2003. Seismic evidence for widespread serpentinized forearc upper mantle along the Cascadia margin. Geology 31, 267–270.

Brudzinski, M.R., Allen, R.M., 2007. Segmentation in episodic tremor and slip all along Cascadia. Geology 35, 907–910. https://doi.org/10.1130/G23740A.1.

Burdick, S., Vernon, F.L., Martynov, V., Eakens, J., Cox, T., Tytell Mulder, T., White, M.C., Astiz, G.L., van der Hilst, R.D., 2017. Model update May 2016: Upper mantle heterogeneity beneath North America from travel-time tomography with global and USArray data. Seismological Research Letters 88, 319–325. https://doi.org/10.1785/0220160186.

Cassidy, J.F., Ellis, R.M., 1993. S wave velocity structure fo the Northern Cascadia subduction zone. Journal of Geophysical Research 98, 4407–4421.

Cassidy, J.F., Waldhauser, F., 2003. Evidence for both crust and mantle earthquakes in the subducting Juan de Fuca plate. Geophysical Research Letters 30, 1095. https://doi.org/10.1029/2002GL015511.

Cawood, P.A., Hawkesworth, C.J., 2013. Temporal relations between mineral deposits and global tectonics. Geological Society, London, Special Publications 393, 9–21. https://doi.org/10.1144/SP393.1.

Christensen, N.I., 1984. Pore pressure and oceanic crustal seismic structure. Geophysical Journal of the Royal Astronomical Society 79, 411–424.

Christensen, N.I., 1996. Poisson's ratio and crustal seismology. Journal of Geophysical Research 101, 3139–3156.

Chuang, L., Bostock, M.G., Wech, A.G., Plourde, A., 2017. Plateau subduction, intraslab seismicity, and the Denali (Alaska) volcanic gap. Geology 45, 647–650. https://doi.org/10.1130/G38867.1.

Cox, S.F., 2016. Injection-drive swarm seismicity and permeability enhancement: Implications for dynamics of hydrothermal ore systems in high fluid-flux overpressured faulting regimes - an Invited Paper. Economic Geology 111, 559–587. https://doi.org/10.2113/econgeo.111.3.559.

Crosson, R.S., 1981. Review of seismicity in the puget sound region from 1970 through 1978: A brief summary. In: Yount, J.C. (Ed.), Earthquake Hazards of the Puget Sound Region, Washington State. USGS Open File Report, Menlo Park, California.

Dahm, T., Fischer, T., 2014. Velocity ratio variations in the source region of earthquake swarms in NW Bohemia obtained from arrival time double differences. Geophysical Journal International 196, 957–970. https://doi.org/10.1093/gji/ggt410.

Doi, I., Noda, S., Iio, Y., Horiuchi, S., Sekiguchi, S., 2013. Relationship between hypocentral distributions and Vp/Vs ratio structures inferred from dense seismic array data: a case study of the 1984 western Nagano Prefecture earthquake, Central Japan. Geophysical Journal International 195, 1323–1336. https://doi.org/10.1093/gji/gg2312.

Dragert, H., Wang, K., 2011. Temporal evolution of an episodic tremor and slip event along the northern Cascadia margin. Journal of Geophysical Research 116, B12406. https://doi.org/10.1029/2011JB008609.

Dragert, H., Wang, K., James, T.S., 2001. A silent slip event on the deeper Cascadia subduction interface. Science 292, 1525–1528. https://doi.org/10.1126/science.1060152.

Evans, B.W., 2008. Control of the products of serpentinization by the Fe2+Mg1 exchange potential of olivine and orthopyroxene. Journal of Petrology 49, 1873–1887. https://doi.org/10.1093/petrology/egn050.

Fisher, D.M., Brantley, S.L., Everett, M., Dzvonik, J., 1995. Cyclic fluid flow through a regionally extensive fracture network within the Kodiak accretionary prism. Journal of Geophysical Research 100, 12881–12894. https://doi.org/10.1029/94JB02816.

Frohlich, C., 1989. The nature of deep-focus earthquakes. Annual Review of Earth and Planetary Sciences 17, 227–254. https://doi.org/10.1146/annurev.ea.17.050189.00103.

Fyfe, W.S., McBirney, A.R., 1975. Subduction and the structure of andesitic volcanic belts. American Journal of Science 275-A, 285–297.

Gao, X., Wang, K., 2014. Strength of stick-slip and creeping subdution meegathrusts from heat flow observations. Science 345, 1038. https://doi.org/10.1126/science.1255487.

Gao, D., Wang, K., Davis, E.E., Jiang, Y., Insua, T.L., He, J., 2017. Thermal state of the Explorere segment of the Cascadia seduction zone: Implications for seismic and tsunami hazards. Geochemistry, Geophysics, Geosystems 18, 1569–1579. https://doi.org/10.1002/2017GC006838.

Geological Survey of Canada, 1989. Canadian national seismograph network. International Federation of Digital Seismograph Networks https://doi.org/10.7914/SN/CN (Other/Seismic Network).
Goldfarb, R.J., Groves, D.I., 2015. Orogenic gold: Common or evolving fluid and metal sources through time. Lithos 233, 2–26. https://doi.org/10.1016/j.lithos.2015.07.011.
Guffanti, M., Weaver, C.S., 1988. Distribution of late Cenozoic volcanic vents in the Cascade range: Volcanic arc segmentation and regional tectonic considerations. Journal of Geophysical Research 93, 6513–6529.
Hacker, B., 1996. Eclogite formation and the rheology, buoyancy, seismicity, and H_2O content of oceanic crust. In: Bebout, G.E., et al. (Eds.), Subduction: Top to Bottom. Geophys. Monogr. Ser Vol. 96. AGU, Washington, D.C., pp. 337–346. https://doi.org/10.1029/GM096p0337.
Hacker, B.R., Peacock, S.M., Abers, G.A., Holloway, S.D., 2003. Subduction factory 2. Are intermediate-depth earthquakes in subducting slabs linked to metamorphic dehydration reactions? Journal of Geophysical Research 108, B12030. https://doi.org/10.1029/2001JB001129.
Halpaap, F., Rondenay, S., Ottemoller, L., 2018. Seismicity, deformation, metamorphism in the Western Hellenic Subduction Zone: New constraints from tomography. Journal of Geophysical Research 123, 3000–3026. https://doi.org/10.1002/2017JB015154.
Hansen, R.T.J., Bostock, M.G., Christensen, N.I., 2012. Nature of the low velocity zone in Cascadia from receiver function waveform inversion. Earth and Planetary Science Letters 337–338, 25–38. https://doi.org/10.1016/j.epsl.2012.05.031.
Hansen, S.M., Schmandt, B., Levander, A., Kiser, E., Vidale, J.E., Abers, G.A., Creager, K.C., 2016. Seismic evidence for a cold serpentinized mantle wedge beneath Mount St Helens. Nature Communications 7, 13242. https://doi.org/10.1038/ncomms13242.
Heaton, T.H., Kanamori, H., 1984. Seismic potential associated with subduction in the northwestern United States. Bulletin of the Seismological Society of America 74, 933–941.
Heinicke, J., Fischer, T., Gaupp, R., Gotze, J., Koch, U., Konietzky, H., Stanek, K.-P., 2009. Hydrothermal alteration as a trigger mechanism for earthquake swarms: the Vogtland/NW Bohemia region as a case study. Geophysical Journal International 178, 1–13.
Hildreth, W., 2007. Quaternary Volcanism in the Cascades – Geological Perspectives. United States Geological Survey Professional Paper 1744.
Houston, H., 2015. Low friction and fault weakening revealed by rising sensitivity of tremor to tidal stress. Nature Geoscience 8, 409–415. https://doi.org/10.1038/ngeo2419.
Hyndman, R.D., 1988. Dipping seismic reflectors, electrically conductive zones and trapped water in the crust over a conducting plate. Journal of Geophysical Research 93, 13391–13405.
Hyndman, R.D., Peacock, S.M., 2003. Serpentinization of the forearc mantle. Earth and Planetary Science Letters 212, 417–432.
Hyndman, R.D., Wang, K., 1993. Thermal constraints on the zone of major thrust earthquake failure: the Cascadia subduction zone. Journal of Geophysical Research 98, 2039–2060.
Hyndman, R.D., Riddihough, R.P., Herzer, R., 1979. The Nootka fault zone – a new plate boundary off western Canada. Geophysical Journal International 58, 667–683. https://doi.org/10.1111/j.1365-246X.1979.tb04801.x.
Hyndman, R.D., Yorath, C.J., Clowes, R.M., Davis, E.E., 1990. The northern Cascadia subduction zone at Vancouver Island: seismic structure and tectonic history. Canadian Journal of Earth Sciences 27, 313–329.
Hyndman, R.D., McCrory, P.A., Wech, A.G., Kao, H., Ague, J., 2015. Cascadia subducting plate fluids channelled to forearc mantle corner: ETS and silica deposition. Journal of Geophysical Research. Solid Earth 120, 4344–4358. https://doi.org/10.1002/2015JB011920.
Ide, S., 2012. Variety and spatial heterogeneity of tectonic tremor worldwide. Journal of Geophysical Research 117, B03302. https://doi.org/10.1029/2011JB008840.
Janiszewski, H.A., Abers, G.A., 2015. Imaging the plate interface in the Cascadia seismogenic zone: new constraints from offshore receiver functions. Seismological Research Letters 86, 1261–1269.
Kao, H., Wang, K., Chen, R.-Y., Wada, I., He, J., Malone, S.D., 2008. Identifying the rupture plane of the 2001 Nisqually, Washington earthquake. Bulletin of the Seismological Society of America 98, 1546–1558. https://doi.org/10.1785/0120070160.
Kao, H., Shan, S.J., Dragert, H., Rogers, G., 2009. Northern Cascadia episodic tremor and slip: A decade of tremor observations from 1997 to 2007. Journal of Geophysical Research 114, 1–20. https://doi.org/10.1029/2008JB006046.
Katayama, I., Kawano, S., Okazaki, K., 2011. Permeability anisotropy of serpentinite and fluid pathways in a subduction zone. Geology 39, 939–942. https://doi.org/10.1130/G32173.1.
Kato, A., Sakai, S., Iidaka, T., Iwasaki, T., Hirata, N., 2010. Non-volcanic seismic swarms triggered by circulating fluids and pressure fluctuations above a solidified diorite intrusion. Geophysical Research Letters 37, L15302. https://doi.org/10.1029/2010GL043887.
Kirby, S., Endgahl, E.R., Denlinger, R., 1996. Intermediate-depth intraslab earthquakes and arc volcanism as physical expressions of crustal and uppermost mantle metamorphism in subducting slabs. In: Bebout, G.E. (Ed.), Subduction: Top to Bottom. Geophysical Monograph Series vol. 96. American Geophysical Union, Washington, DC, pp. 195–214. https://doi.org/10.1029/GM096p0195.
Kirby, S.H., Wang, K., Brocher, T.M., 2014. A large mantle water source for the northern San Andreas fault system: a ghost of subduction past. Earth, Planets and Space 66, 67. https://doi.org/10.1186/1880-5981-66-67.
Li, G., Liu, Y., Regalla, C., Morell, K., 2018. Seismicity relocation and fault structure near the Leech River Fault Zone, southern Vancouver Island. Journal of Geophysical Research 123, 2841–2855. https://doi.org/10.1002/2017JB015021.
Lin, Y., Shearer, P.M., 2009. Evidence for water-filled cracks in earthquake source regions. Geophysical Research Letters 36, L17315. https://doi.org/10.1029/2009GL039098.
Ludwin, R.S., Weaver, C.S., Crosson, R.S., 1991. Seismicity of Washington and Oregon. In: Slemmons, D.B., Engdahl, E.R., Zoback, M.D., Blackwell, D. (Eds.), Neotectonics of North America, Decade Map Volume 1. The Geological Society of America, Boulder, Colorado, pp. 77–98.
Malvoisin, B., Brantut, N., Kaczmarek, M.-A., 2017. Control of serpentinization rate by reaction-induced cracking. Earth and Planetary Science Letters 476, 143–152. https://doi.org/10.1016/j.epsl.2017.07.042.
Mann, M.E., Abers, G.A., Creager, K.C., Ulberg, C.W., Crosbie, K., 2017. Array-Based Receiver Function Analysis of the Subducting Juan de Fuca plate Beneath the Mount St Helens Region and its Implications for Subduction Geometry and Metamorphism, T42C-08, Presented at 2017. AGU Fall Meeting, New Orleans, Louisiana, U.S.A, pp. 11–15 December.
McCrory, P.A., Blair, J.L., Waldhauser, F., Oppenheimer, D.H., 2012. Juan de Fuca slab geometry and its relation to Wadati-Benioff zone seismicity. Journal of Geophysical Research 117, B09306. https://doi.org/10.1029/2012JB009407.
McCrory, P.A., Constantz, J.E., Hunt, A.G., Blair, J.L., 2016. Helium as a tracer for fluids released from Juan de Fuca lithosphere beneath the Cascadia forearc. Geochemistry, Geophysics, Geosystems 17, 2825–2834. https://doi.org/10.1002/2016GC006406.
McGary, R.S., Evans, R.L., Wannamaker, P.E., Eisenbeck, J., Rondenay, S., 2014. Pathway from subducting slab to surface for melt and fluids beneath Mount Rainier. Nature 511, 338–340. https://doi.org/10.1038/nature13493.
Merrill, R., Bostock, M.G., 2018. An Earthquake Nest in Cascadia, S11D-0389, Presented at 2018. AGU fall meeting, Washington, D.C., pp. 10–14 December.
Moody, J.B., 1976. Serpentinization: a review. Lithos 9, 125–138.
Morell, K.D., Regalla, C., Leonard, L.J., Amos, C., Levson, V., 2017. Quaternary rupture of a crustal fault beneath Victoria, British Columbia, Canada. GSA Today 27, 4–10. https://doi.org/10.1130/GSATG291A.1.
Nedimovic, M.R., Hyndman, R.D., Kumar, R., Spence, G.D., 2003. Reflection signature of seismic and aseismic slip on the northern Cascadia subduction interface. Nature 424, 416–420.
Nicholson, T., Bostock, M.G., Cassidy, J.F., 2005. New constraints on subduction zone structure in northern Cascadia. Geophysical Journal International 1613, 849–859. https://doi.org/10.1111/j.1365-246X.2005.02605.x.
Obana, K., Scherwath, M., Yamamoto, Y., Kodaira, S., Wang, K., Spence, G., Riedel, M., Kao, H., 2014. Earthquake activity in northern Cascadia subduction zone off Vancouver Island revealed by ocean-bottom seismograph observations. Bulletin of the Seismological Society of America 105, 489–495. https://doi.org/10.1785/0120140095.
Obara, K., 2002. Nonvolcanic deep tremor associated with subduction in Southwest Japan. Science 296, 1679–1681. https://doi.org/10.1126/science.1070378.
Obrebski, M., Allen, R.M., Xue, M., Hung, S.-H., 2010. Slab-plume interaction beneath the Pacific Northwest. Geophysical Research Letters 37, L14305. https://doi.org/10.1029/2010GL043489.
O'Hanley, D.S., 1992. Solution to the volume problem in serpentinization. Geology 20, 705–708.
Peacock, S.M., 1993. Large-scale hydration of the lithosphere above subducting slabs. Chemical Geology 108, 49–59.
Peacock, S.M., 2001. Are the lower planes of double seismic zones caused by serpentine dehydration in subducting oceanic mantle? Geology 29, 299–302. https://doi.org/10.1130/0091-7613.
Peacock, S.M., 2009. Thermal and metamorphic environment of subduction zone episodic tremor and slip. Journal of Geophysical Research 114, B00A07. https://doi.org/10.1029/2008JB005978.
Peacock, S.M., Wang, K., 1999. Seismic consequences of warm versus cool subduction metamorphism: examples from southwest and Northeast Japan. Science 286, 937–939.
Peacock, S.M., Christensen, N.I., Bostock, M.G., Audet, P., 2011. High pore pressures and porosity at 35 km depth in the Cascadia subduction zone. Geology 39, 471–474. https://doi.org/10.1130/G31649.1.
Peterson, C.L., Christensen, D.H., 2009. Possible relationship between non-volcanic tremor and the 1998-2001 slow slip event, south Central Alaska. Journal of Geophysical Research 114, B06302. https://doi.org/10.1029/2008JB/006096.
Plourde, A.P., Bostock, M.G., Audet, P., Thomas, A.M., 2015. Low-frequency earthquakes at the southern Cascadia margin. Geophysical Research Letters 42, 4849–4855.
Preston, L.A., Creager, K.C., Crosson, R.S., Brocher, T.M., Trehu, A.M., 2003. Intraslab earthquakes: dehydration of the Cascadia slab. Science 302, 1197–1200.
Ramachandran, K., Hyndman, R.D., 2012. The fate of fluids released from subducting slab in northern Cascadia. Solid Earth 3, 121–129. https://doi.org/10.5194/se-3-121-2012.
Riddihough, R.P., 1977. A model for recent plate interactions off Canada's west coast. Canadian Journal of Earth Sciences 14, 384–396. https://doi.org/10.1139/e77-039.
Riddihough, R.P., Hyndman, R.D., 1976. Canada's active western margin – the case for subduction. Geoscience Canada 3, 269–278.
Rogers, G.C., 1983. Seismotectonics of British Columbia. Ph.D Thesis. The University of British Columbia.
Rogers, G.C., 1985. Variation in Cascade volcanism with margin orientation. Geology 13, 4995–4998. https://doi.org/10.1130/0091-7613(198513<495:VICVWM>2.0.CO;2.
Rogers, G.C., 1988. An assessment of the megathrust earthquake potential of the Cascadia subduction. Canadian Journal of Earth Sciences 25, 844–852. https://doi.org/10.1139/e88-083.
Rogers, G., Dragert, H., 2003. Episodic tremor and slip on the Cascadia subduction zone: the chatter of silent slip. Science 300, 1942–1943. https://doi.org/10.1126/science.1084783.
Rogers, G.C., Horner, R.B., 1991. An overview of western Canadian seismicity. In: Slemmons, D.B., Engdahl, E.R., Zoback, M.D., Blackwell, D. (Eds.), Neotectonics of North America, Decade Map Volume 1. The Geological Society of America, Boulder, Colorado, pp. 127–130.

Rondenay, S., Bostock, M.G., Shragge, J., 2001. Multiparameter two-dimensional inversion of scattered teleseismic body waves 3. Application to the Cascadia 1993 data set. Journal of Geophysical Research 106, 30795–30807.
Rondenay, S., Abers, G.A., van Keken, P.E., 2008. Seismic imaging of subduction zone metamorphism. Geology 36, 275–278.
Rondenay, S., Montesi, L.G.J., Abers, G.A., 2010. New geophysical insight into the origin of the volcanic gap. Geophysical Journal International 182, 613–630. https://doi.org/10.1111/j.1365-246X.2010.04659.x.
Royer, A.A., Bostock, M.G., 2014. A comparative study of low frequency earthquake templates in northern Cascadia. Earth and Planetary Science Letters 402, 247–256. https://doi.org/10.1016/j.epsl.2013.08.040.
Royer, A.A., Thomas, A.M., Bostock, M.G., 2014. Tidal Modulation and Triggering of Low-Frequency Earthquakes in Northern Cascadia. Vol. 120, pp. 384–405. https://doi.org/10.1002/2014JB011430.
Rubinstein, J.L., Gomberg, J., Vidale, J.E., Wech, A.G., Kao, H., Creager, K.C., Rogers, G., 2009. Seismic wave triggering of nonvolcanic tremor, episodic tremor and slip, and earthquakes on Vancouver Island. Journal of Geophysical Research 114, B00A01. https://doi.org/10.1029/2008JB005875.
Rudge, J.F., Kelemen, P.B., Spiegelman, M., 2010. A simple model of reaction-induced cracking applied to serpentinization and carbonation of peridotite. Earth and Planetary Science Letters 291, 215–227. https://doi.org/10.1016/j.epsl.2010.01.016.
Satake, K., Shimazaki, K., Tsuji, Y., Ueda, K., 1996. Time and size of a prehistoric great earthquake in the Cascadia subduction zone as inferred from Japanese tsunami records dated January 1700. Nature 379, 246–249.
Savard, G., 2018. Seismic Velocity Structure Under Vancouver Island From Travel Time Inversion: Insight From Low Frequency Earthquakes. (Doctoral thesis). Retrieved from. https://circle.ubc.ca/.
Savard, G., Bostock, M.G., Christensen, N.I., 2018. Seismicity, metamorphism, and fluid evolution across the northern Cascadia forearc. Geochemistry, Geophysics, Geosystems https://doi.org/10.1029/2017GC007417 (in press).
Scholz, C.H., 2002. Mechanics of Earthquakes and Faulting. Cambridge University Press, Cambridge, U.K.
Shelly, D.R., Beroza, G.C., Ide, S., Nakamula, S., 2006. Low-frequency earthquakes in Shikoku, Japan, and their relationship to episodic tremor and slip. Nature 442, 188–191.
Sherrod, D.R., Smith, J.G., 1990. Quaternary extrusion rates of the Cascade Range, northwestern United States and southern British Columbia. Journal of Geophysical Research 95, 19456–19474. https://doi.org/10.1029/JB095iB12p19465.
Sibson, R.H., Robert, F., Poulsen, H.K., 1988. High-angle reverse faults, fluid-pressure cycling and mesothermal gold-quartz deposits. Geology 16, 551–555.
Spence, W., 1987. Slab pull and the seismotectonics of subducting lithosphere. Reviews of Geophysics 25, 55–69. https://doi.org/10.1029/RG025i001p00055.
Spence, W., 1989. Stress origins and earthquake potentials in Cascadia. Journal of Geophysical Research 94, 3076–3088.
Stone, I., Vidale, J.E., Han, S., Roland, E., 2018. Catalog of offshore seismicity in Cascadia: insights into the regional distributionof microseismicity and its relation to subduction processes. Journal of Geophysical Research 123, 641–652. https://doi.org/10.1002/2017JB014966.
Takei, Y., 2002. Effect of pore geometry on Vp/Vs: From equilibrium geometry to crack. Journal of Geophysical Research 107 (B2), 2043. https://doi.org/10.1029/2001JB000522.
Thomas, A.M., Bostock, M.G., 2015. Identifying low-frequency earthquakes in Central Cascadia using cross-station correlation. Tectonophysics 658, 111–116. https://doi.org/10.1016/j.tecto.2015.07.013.
Trehu, A.M., Braunmiller, J., Nabelek, J.L., 2008. Probable low-angle thrust earthquakes on the Juan de Fuca – North America plat boundary. Geology 36, 127–130. https://doi.org/10.1130/G24145A.1.
Ulmer, P., Trommsdorff, V., 1995. Serpentine stability to mantle depths and subduction-related magmatism. Science 268, 858–861.
Uhrhammer, R.A., 1991. Northern California seismicity. In: Slemmons, D.B., Engdahl, E.R., Zoback, M.D., Blackwell, D. (Eds.), Neotectonics of North America, Decade Map Volume 1. The Geological Society of America, Boulder, Colorado, pp. 99–106.
University of Washington, 1963. Pacific Northwest Seismic network. International Federation of Digital Seismograph Networks https://doi.org/10.7914/SN/UW (Other/Seismic Network).
USGS Menlo Park, 1967. USGS Northern California network. International Federation of Digital Seismograph Networks https://doi.org/10.7914/SN/NC (Other/Seismic Network).
Vidale, J.E., Shearer, P.M., 2006. A survey of 71 earthquake bursts across southern California: Exloring the role of pore fluid pressure fluctuations and aseismic slip as drivers. Journal of Geophysical Research 111, B05312. https://doi.org/10.1029/2005JB004034.
Vidale, J.E., Schmidt, D.A., Malone, S.D., Hotovec-Ellis, A.J., Moran, S.C., Creager, K.C., Houston, H., 2014. Deep long-period earthquakes west of the volcanic arc in Oregon: evidence of serpentine dehydration in the fore-earc mantle wedge. Geophysica. Research Letters 41, 370–376. https://doi.org/10.1002/2013GL059118.
Wada, I., Mazzotti, S., Wang, K., 2010. Intraslab stresses in the Cascadia subduction zone from inversion of earthquake focal mechanisms. Bulletin of the Seismological Society of America 100, 2002–2013. https://doi.org/10.1785/0120090349.
Weaver, C.S., Baker, G.E., 1988. Geometry of the Juan de Fuca plate beneath Washington – evidence from seismicity and the 1949 South Puget sound earthquake. Bulletin of the Seismological Society of America 78, 264–275.
Wech, A.G., 2010. Interactive tremor monitoring. Seismological Research Letters 81, 664–669. https://doi.org/10.1785/gssrl.81.4.664.
Wech, A.G., 2016. Extending Alaska's plate boundary: tectonic tremor generated by Yakutat subduction. Geology 44, 590–597. https://doi.org/10.1130/G37817.1.
Wells, R.E., Blakely, R.J., Wech, A.G., McCrory, P.A., Michael, A., 2017. Cascadia subduction tremor muted by crustal faults. Geology 45, 515–518. https://doi.org/10.1130/G38835.1.
Zhang, H., Thurber, C.H., 2003. Double-difference tomography: the method and its application to the Hayward Fault, California. Bulletin of the Seismological Society of America 93, 1875–1889. https://doi.org/10.1785/0120020190.